Mon. Not. R. Astron. Soc. **000**, 1–5 (2015) Printed 31 December 2015 (MN LATEX style file v2.2)

NIHAO VII: Predictions for the galactic baryon budget in dwarf to Milky Way mass haloes

Liang Wang[1,3⋆], Aaron A. Dutton[2,3], Gregory S. Stinson[3], Andrea V. Macciò[2,3], Thales Gutcke[3], Xi Kang[1]
[1] *Purple Mountain Observatory, the Partner Group of MPI für Astronomie, 2 West Beijing Road, Nanjing 210008, China*
[2] *New York University Abu Dhabi, PO Box 129188, Abu Dhabi, UAE*
[3] *Max-Planck-Institut für Astronomie, Königstuhl 17, 69117 Heidelberg, Germany*

to be submitted to MNRAS

ABSTRACT
We use the NIHAO galaxy formation simulations to make predictions for the baryonic budget in present day galaxies ranging from dwarf ($M_{\rm tot} \sim 10^{10}{\rm M}_\odot$) to Milky Way ($M_{\rm tot} \sim 10^{12}{\rm M}_\odot$) masses. The sample is made of 88 independent high resolution cosmological zoom-in simulations. NIHAO galaxies reproduce key properties of observed galaxies, such as the stellar mass vs halo mass and cold gas vs stellar mass relations. Thus they make plausible predictions for the baryon budget. We present the mass fractions of stars, cold gas ($T < 10^4$K), cool gas ($10^4 < T < 10^5$K), warm-hot gas ($10^5 < T < 10^7$K), and hot gas (10^7K$< T$), inside the virial radius, R_{200}. Compared to the predicted baryon mass, using the dark halo mass and the universal baryon fraction, $f_{\rm b} \equiv \Omega_{\rm b}/\Omega_{\rm m} = 0.15$, we find that for all of our haloes, the missing mass is not just outside the virial radius $R_{\rm vir}$, it has been relocated past $2R_{\rm vir}$. Haloes of mass $M_{\rm tot} \sim 10^{10}{\rm M}_\odot$ are missing $\sim 90\%$ of their baryons. More massive haloes ($M_{\rm tot} \sim 10^{12}{\rm M}_\odot$) retain a higher fraction of their baryons, with $\sim 30\%$ missing, consistent with observational estimates.

Key words: galaxies: evolution – galaxies: formation – galaxies: dwarf – galaxies: spiral – methods: numerical – cosmology: theory

1 INTRODUCTION

Cosmic structure formation has redistributed the baryons from a nearly uniformly distributed plasma into a variety of states, including stars, stellar remnants, cold (atomic and molecular) gas, and hot (ionized) gas. The theories of galaxy formation can predict the amount of mass in these different states, which can in turn be tested by observational constraints.

On cosmological scales, the ratio between the total baryonic and gravitating mass is measured to be $f_{\rm b} \equiv \Omega_{\rm b}/\Omega_{\rm m} \simeq 0.16$ (The Planck Collaboration 2014). However, the cold baryonic mass density implied by several galaxy baryon estimates is only 3-8% of the big bang nucleosynthesis expection (Persic & Salucci 1992; Fukugita et al. 1998; Bell et al. 2003; McGaugh et al. 2010). The majority of the cosmic baryons are thought to be in the form of hot gas around or between galaxies (Cen & Ostriker 1999). Until recently only a fraction of these baryons had been detected (Bregman 2007; Shull et al. 2012). This discrepancy is referred to as the "missing baryon problem". Recent advances in the detection of gas in the circum galactic medium (CGM) have come from the COS survey (Tumlinson et al. 2011, 2013; Thom et al. 2012; Werk et al. 2012, 2013). On the scale of Milky Way mass haloes $M_{\rm tot} \sim 10^{12}{\rm M}_\odot$ a significant amount of warm ($10^4 < T < 10^7$K) gas has been detected (Werk et al. 2014), accounting for 33-88% of the baryon budget. In the future such observations will be extended to a wider range of halo masses.

In this paper we make predictions for the baryonic budget for stars, cold, warm and hot gas in and around the virial radius of haloes of mass ranging from $M_{\rm tot} \sim 10^{10}{\rm M}_\odot$ to $10^{12}{\rm M}_\odot$. We use a sample of 88 zoom-in galaxy formation simulations from the NIHAO project. NIHAO galaxies are consistent with the stellar mass vs halo mass relations from halo abundance matching since redshift $z \sim 4$ (Wang et al. 2015), the galaxy star formation rate vs stellar mass relation since $z \sim 4$ (Wang et al. 2015), and the cold gas mass vs stellar mass relation at $z \sim 0$ (Stinson et al. 2015). Therefore, the simulations make plausible predictions for the mass fractions and physical locations of the warm and hot gas components. We find that all the haloes contain less baryons than expected according to the cosmic baryonic fraction, but the missing fraction is strongly mass dependent.

⋆ lwang@mpia.de

This paper is organized as follows: The cosmological hydrodynamical simulations including star formation and feedback are briefly described in §2; In §3 we present the results including the baryonic budget, baryon distribution, and a comparison with observations; §4 gives a summary of our results.

2 SIMULATIONS

In this study we use simulations from the NIHAO (Numerical Investigation of a Hundred Astrophysical Objects) project (Wang et al. 2015). The initial conditions are created to keep the same numerical resolution across the whole mass range with typically a million dark matter particles inside the virial radius of the target halo at redshift $z = 0$. The halos to be re-simulated at higher resolution with baryons have been extracted from 3 different pure N-body simulations with a box size of 60, 20 and 15 h^{-1} Mpc respectively. We adopted the latest compilation of cosmological parameters from the Planck satellite (the Planck Collaboration et al. 2014). More information on the collisionless parent simulations and sample selection can be found in Dutton & Macciò (2014) and Wang et al. (2015)

We use the SPH hydrodynamics code GASOLINE (Wadsley et al. 2004), with a revised treatment of hydrodynamics as described in Keller et al. (2014). The code includes a subgrid model for turbulent mixing of metal and energy (Wadsley et al. 2008), heating and cooling include photoelectric heating of dust grains, ultraviolet (UV) heating and ionization and cooling due to hydrogen, helium and metals (Shen et al. 2010). The star formation and feedback modeling follows what was used in the MaGICC simulations (Stinson et al. 2013). There are two small changes in NIHAO simulations: The change in number of neighbors and the new combination of softening length and particle mass increases the threshold for star formation from 9.3 to 10.3 cm^{-3}, the increase of pre-SN feedback efficiency $\epsilon_{\rm ESF}$, from 0.1 to 0.13. The more detail on star formation and feedback modeling can be found in Wang et al. (2015).

3 BARYON BUDGET

We define the fiducial baryonic mass as:

$$M_{\rm b} \equiv M_{\rm b}(R_{200}) = \frac{f_{\rm b}}{1-f_{\rm b}} M_{\rm dm}(R_{200}) \qquad (1)$$

where the $M_{\rm dm}$ is the total dark matter mass in the halo, and the $f_{\rm b} = \Omega_{\rm b}/\Omega_{\rm m} \sim 0.15$ is the cosmic baryon fraction (the ratio between baryon density and mass density including baryonic mass plus dark matter), so that the $M_{\rm b}$ is the baryonic mass inside the virial radius if the baryons follow the dark matter closely.

Fig. 1 shows the ratio between the mass of each baryon component inside the virial radius to the fiducial baryonic mass for the most massive galaxy in each zoom-in region. We present the fractions of total stellar mass (blue points), and the total baryonic mass including stellar mass plus gas mass (green points). For the stellar mass fraction we also show the relations from the halo abundance matching (Moster et al. 2013; Behroozi et al. 2013; Kravtsov et al. 2014). The grey

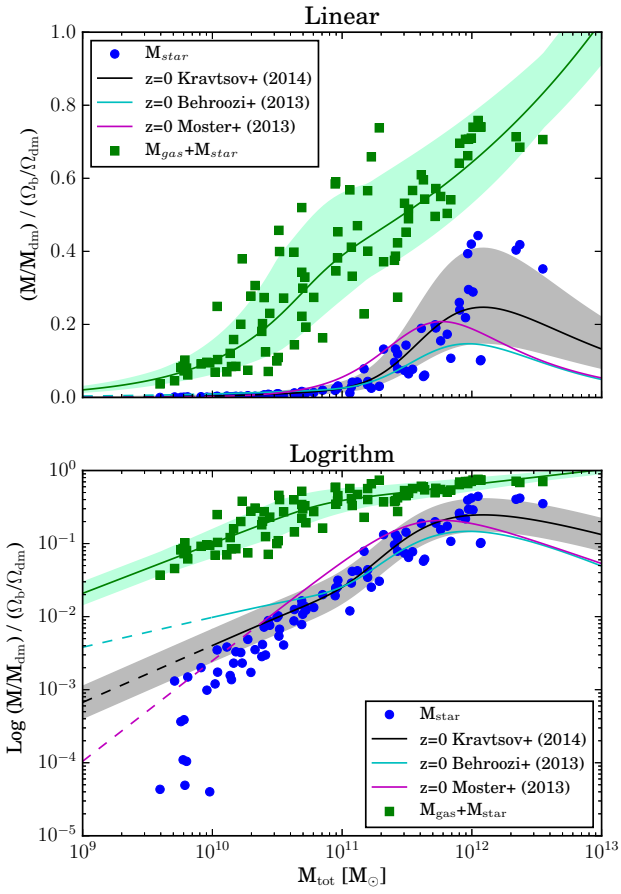

Figure 1. Fractional baryon content of our NIHAO simulations as a function of halo mass. The green points show the ratio between the baryonic mass (stars + gas) inside the virial radius and the total baryonic mass associated with the dark matter halo and the green lines are best fitting lines. The blue points show the corresponding fraction for the stars. The solid green line and shaded region shows a double power-law fit, together with the 1σ scatter. For the stellar mass fraction we show several relations from halo abundance matching. The linear (upper panel) and logarithmic (lower panel) scales emphasize the large amount of "missing" baryons and the low star formation efficiencies.

area is the one sigma scatter around the mean value from Kravtsov et al. (2014).

We tried to capture the behaviour of the baryonic mass fraction as a function of the halo mass using a double power law formula:

$$\frac{f}{f_0} = \left(\frac{M_{200}}{\mathcal{M}_0}\right)^{\alpha} \left\{0.5\left[1+\left(\frac{M_{200}}{\mathcal{M}_0}\right)^{\gamma}\right]\right\}^{\frac{\beta-\alpha}{\gamma}}. \qquad (2)$$

In this formula, the lower and higher mass ends have logarithmic slope α and β, respectively, while γ regulates how sharp the transition is from the lower to the higher ends. The best fit parameters are as follows:

$$\mathcal{M}_0 = 6.76 \times 10^{10}$$
$$f_0 = 0.336$$

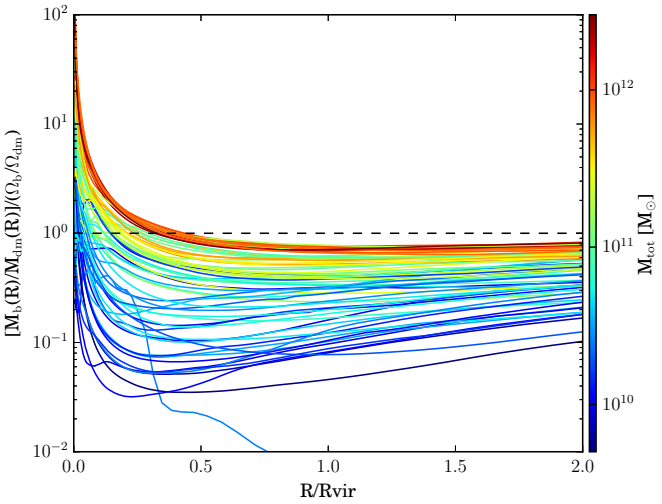

Figure 2. Baryon distribution of each galaxy from NIHAO simulations. A comparison of how the baryons distribute in the halo with different masses. The lines are color coded by their halo mass, which show a clear trend that the more massive halo preserve more baryons alone the radius.

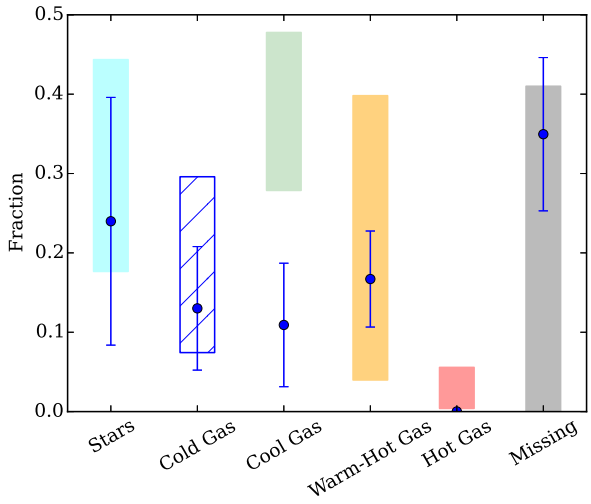

Figure 3. Baryonic budget (the fraction of different components) of $3.5 \times 10^{11} < M_{200}/\mathrm{M}_\odot < 3.5 \times 10^{12}$ NIHAO galaxies (blue points with 1σ error bars) compared with observations of $\mathrm{M}_{200} = 10^{12.2}$ $\mathrm{M}_\odot$ galaxies (shaded regions)

Table 1. Scatters for best fit parameters for the total baryonic mass fraction computed inside one virial radius, R_{200}, as a function of halo mass M_{200} in different mass ranges.

Mass Range	σ
$3 \times 10^9 \mathrm{M}_\odot < \mathrm{M}_{200} < 2 \times 10^{10} \mathrm{M}_\odot$	0.151
$2 \times 10^{10} \mathrm{M}_\odot < \mathrm{M}_{200} < 7 \times 10^{10} \mathrm{M}_\odot$	0.236
$7 \times 10^{10} \mathrm{M}_\odot < \mathrm{M}_{200} < 3 \times 10^{11} \mathrm{M}_\odot$	0.125
$3 \times 10^{11} \mathrm{M}_\odot < \mathrm{M}_{200} < 3.5 \times 10^{12} \mathrm{M}_\odot$	0.0518

$$\begin{aligned} \alpha &= 0.684 \\ \beta &= 0.205 \\ \gamma &= 3.40 \end{aligned} \quad (3)$$

The green shaded region indicates the scatter about the best fit line. These are measured in four different mass ranges, and are summarized in Table. 1.

The trends of each component fraction are similar, in that the fractions are relatively low in low mass haloes, and increase as the halo mass increases. The main difference between the different components is the slope, with the baryonic mass fraction having a shallower slope than the stellar mass fraction. This is because in low mass haloes ($M_{\rm tot} \sim 10^{10} \mathrm{M}_\odot$) most of the baryons are in the form of gas, while in the highest mass haloes we study ($M_{\rm tot} \sim 10^{12} \mathrm{M}_\odot$) there are roughly equal amounts of stars and gas.

Fig. 1 shows that all haloes in our study contain less than the universal fraction of baryons. The upper panel uses a linear y-axis scale, which highlights the large amount of baryons that are missing, especially in low mass haloes. The logarithmic scale in the lower panel highlights the power-law nature of the relatons.

Since the haloes we study are above the mass where the cosmic UV background prevents gas from cooling, the missing baryons have most likely been ejected from the central galaxies in supernova/stellar feedback driven winds. Although the lower mass galaxies have converted a smaller fraction of their available baryons into stars, and hence there is proportionally less energy available to drive an outflow, they have expelled a larger fraction of their baryons, consistent with expectations from energy driven gas outflows (e.g., Dutton 2012).

3.1 Where are the missing baryons?

Fig. 2 shows the mass ratio profiles of total baryons for each simulation. Here the y-axis is the ratio between the baryonic to dark matter mass, $M_{\rm b}(< R)/M_{\rm dm}(< R)$, enclosed within a sphere of radius, R, normalized by the cosmic baryon-to-dark matter ratio, $\Omega_{\rm b}/\Omega_{\rm dm}$.

Each solid curve represents a halo, and the curves are colored by their halo mass (red for high masses to blue for low masses). Broadly speaking, the curves have a similar shape, with a normalization that depends on halo mass. They have a cusp in the central region where the stars and cold gas dominate, then become flat in the outer region. More massive haloes have higher baryon fractions at all radii. At small radii, the baryon to dark matter ratio is higher than the cosmic value due to gas dissipation. Even beyond the virial radius, there is little change in the baryon fraction up to 2 virial radii. We thus conclude that the missing baryons are well outside of the virial radius.

3.2 Comparison with Observations of Milky Way mass haloes

Since the CGM is too diffuse to create emission lines, it must be observed using quasar absorption lines. The COS-HALOs survey is filling in details about the $z \sim 0$ CGM (Peeples et al. 2014; Tumlinson et al. 2011, 2013; Werk et al. 2012, 2013, 2014). For the CGM of low-redshift L^* galaxies, Tumlinson et al. (2013) and Peeples et al. (2014) constrain the mass of the warm-hot CGM ($T \sim 10^{5-7}$), Werk et al. (2014) provides a strict lower limit to the mass of cool material ($T \sim 10^{4-5}$) in the CGM of these galaxies. In a study using X-rays, Anderson et al. (2013) place a constraints on

Table 2. The baryonic budget parameters for galaxies in NIHAO sample in different mass bins. We refer to gas in the temperature range T $< 10^4$ K as cold; 10^4 K $\leqslant$ T $< 10^5$ K as cool; 10^5 K $\leqslant$ T $< 10^7$ K as warm; and T $\geqslant 10^7$ K as hot.

$\langle \log_{10}(M_{200}/\mathrm{M}_\odot) \rangle$	9.992 ± 0.223	10.588 ± 0.143	11.267 ± 0.209	11.963 ± 0.278
$\langle \log_{10}(M_\mathrm{b}/\mathrm{M}_\odot) \rangle$	9.243 ± 0.215	9.829 ± 0.139	10.493 ± 0.206	11.176 ± 0.273
$\langle M_\star/M_\mathrm{b} \rangle$	1.61×10^{-3}	9.57×10^{-3}	6.43×10^{-2}	0.240
$\sigma_\star$	1.63×10^{-3}	4.24×10^{-3}	5.02×10^{-2}	0.156
$\langle M_\mathrm{cold}/M_\mathrm{b} \rangle$	1.37×10^{-2}	3.92×10^{-2}	0.124	0.130
σ_cold	8.24×10^{-3}	4.08×10^{-2}	3.58×10^{-2}	7.78×10^{-2}
$\langle M_\mathrm{cool}/M_\mathrm{b} \rangle$	0.103	0.192	0.203	0.109
σ_cool	7.56×10^{-2}	0.135	0.138	6.37×10^{-2}
$\langle M_\mathrm{warm}/M_\mathrm{b} \rangle$	7.92×10^{-4}	1.48×10^{-2}	5.83×10^{-2}	0.167
σ_warm	1.25×10^{-3}	6.53×10^{-3}	3.19×10^{-2}	6.05×10^{-2}
$\langle M_\mathrm{hot}/M_\mathrm{b} \rangle$	0.000	0.000	0.000	1.82×10^{-4}
σ_hot	0.000	0.000	0.000	2.33×10^{-4}
$\left\langle M_\mathrm{missing}/M_\mathrm{b} \right\rangle$	0.880	0.744	0.548	0.350
σ_missing	5.65×10^{-2}	0.137	0.110	9.66×10^{-2}

the mass of hot gas ($T > 10^7$) residing in the extended hot halos.

In Fig. 3, we show the mean values and standard deviation of the mass fraction of stars and different components of gas in our most massive galaxies ($3.49 \times 10^{11}\mathrm{M}_\odot <$ M$_{200}$ $< 3.53 \times 10^{12}\mathrm{M}_\odot$) with blue points and error bars. The gas is assigned to a range of temperature bins: cold gas (T $< 10^4$ K), cool gas (10^4 K $<$ T $< 10^5$ K), warm gas (10^5 K $<$ T $< 10^7$ K) and hot gas (T $> 10^7$ K). The observational constraints are shown with the same colour scheme in Fig. 11 in Werk et al. (2014).

In this plot Werk et al. (2014) provides observational constraints for CGM gas mass that are shown as the shaded bars. The stellar mass range comes from halo abundance matching as described in Kravtsov et al. (2014). The cold disk gas mass comes from from Dutton et al. (2011).

The observations and the simulations match well in every phase outside of the cool CGM gas, where the observations find 3× the mass that simulations predict. If the observations are correct, the simulations have either ejected too far gas that could be cool, or they have created a CGM with the wrong mix of gas temperatures. The total gas fractions (0.39 in COS-HALOs, 0.41 in NIHAO) suggest the latter option. As the CGM of lower mass galaxies will soon be observed , Table 2 lists information about CGM mass fractions of the different components of gas in haloes down to a halo mass of $\sim 10^{10}\mathrm{M}_\odot$.

4 SUMMARY

We have used the NIHAO galaxy simulation suite (Wang et al. 2015) to study the statistical features of the baryonic budget and distribution spanning halo masses of $\sim 10^{10}$ to $\sim 10^{12}\mathrm{M}_\odot$. NIHAO is a large (currently 88) set of high resolution cosmological hydrodynamical galaxy formation simulations. As shown in previous papers the NIHAO galaxies reproduce several key observed scaling relations. We summarize our results as follows:

- All of the NIHAO haloes have a lower baryon to dark matter ratio, inside the viriral radius, than the cosmic baryon fraction.
- The missing baryons in all haloes are beyond 2 virial radii.
- Lower mass haloes have lost a larger fraction of their baryons, even though they convert a lower fraction of the baryons into stars.
- For the highest mass haloes in our study $\sim 10^{12}\mathrm{M}_\odot$ our simulations are consistent with the observed fractions of stars, cold gas, warm and hot gas. However, we underpredict the cool ($10^4 < T < 10^5 K$) gas with $f_\mathrm{cool} = 0.11 \pm 0.06$ vs 0.28-0.48 observed.
- This discrepancy may indicate that our feedback model pushes the gas too far, or puts gas in the wrong phases, and can be resolved with future observations. Since we match the overall gas fraction we think that there might be some problem in mixing the gas temperature.

ACKNOWLEDGMENTS

GASOLINE was written by Tom Quinn and James Wadsley. Without their contribution, this paper would have been impossible. The simulations were performed on the THEO cluster of the Max-Planck-Institut für Astronomie and the HYDRA cluster at the Rechenzentrum in Garching; and the Milky Way supercomputer, funded by the Deutsche Forschungsgemeinschaft (DFG) through Collaborative Research Center (SFB 881) "The Milky Way System" (subproject Z2), hosted and co-funded by the Jülich Supercomputing Center (JSC). We greatly appreciate the contributions of all these computing allocations. AAD, GSS and AVM acknowledge support through the Sonderforschungsbereich SFB 881 The Milky Way System (subproject A1) of the German Research Foundation (DFG). The analysis made use of the pynbody package (Pontzen et al. 2013). The authors acknowledge support from the MPG-CAS through the partnership programme between the MPIA group lead by AVM and the PMO group lead by XK. LW acknowledges support of the MPG-CAS student programme. XK acknowledge the support from 973 program (No. 2015CB857003, 2013CB834900), NSFC project No.11333008 and the "Strategic Priority Research Program the Emergence of Cosmological Structures" of the CAS(No.XD09010000).

REFERENCES

Anderson, M. E., Bregman, J. N., Dai, X. 2013, ApJ, 762, 106
Agertz, O., Moore, B., Stadel, J. 2007, MNRAS, 380, 963
Behroozi, P. S., Wechsler, R. H., & Conroy, C. 2013, ApJ, 770, 57
Bell, E. F., McIntosh, D. H., Katz, N., Weinberg, M. D., 2003, ApJ, 585, 117
Bregman, J. N. 2007, ARAA, 45, 221
Cen, R. Y., Ostriker, J. P. 1999, ApJ, 514, 1
Dutton, A. A., Conroy, C., van den Bosch, F. C., et al. 2011, MNRAS, 416, 322
Dutton, A. A. 2012, MNRAS, 424, 3123
Dutton, A. A., & Macciò, A. V. 2014, MNRAS, 441, 3359
Fukugita, M., Hogan, C. J., Peebles, P. J. F. 1998, ApJ, 503, 518
Keller, B. W., Wadsley, J., Benincasa, S. M., & Couchman, H. M. P. 2014, MNRAS, 442, 3013
Kravtsov, A., Vikhlinin, A., & Meshscheryakov, A. 2014, arXiv:1401.7329
McGaugh, S. S., Schombert, J. M., de Blok, W. J. G., Zagursky, M. J. 2010, MNRAS, 708, 14
Moster, B. P., Naab, T., & White, S. D. M. 2013, MNRAS, 428, 3121
Planck Collaboration, Ade, P. A. R., Aghanim, N., et al. 2014, A&A, 571, AA16
Peeples, M. S., Werk, J. K., Tumlinson, J., et al. 2014, ApJ, 786, 54
Persic, M., Salucci, P. 1992, MNRAS, 258, 14
Pontzen, A., Roškar, R., Stinson, G., & Woods, R. 2013, Astrophysics Source Code Library, 1305.002
Shen, S., Wadsley, J., & Stinson, G. 2010, MNRAS, 407, 1581
Shull, J. M., Smith, B. D., Danforth, C. W. 2012, ApJ, 759, 23
Stinson, G. S., Brook, C., Macciò, A. V., et al. 2013, MNRAS, 428, 129
Thom, C., Tumlinson, J., Werk, J. K. 2012, ApJL, 758, L41
Tumlinson, J., Thom, C., Werk, J., et al. 2011, Science, 334, 948
Tumlinson, J., Thom, C., Werk, J., et al. 2013, ApJ, 777, 59
Wadsley, J. W., Stadel, J., & Quinn, T. 2004, NewA, 9, 137
Wadsley, J. W., Veeravalli, G., & Couchman, H. M. P. 2008, MNRAS, 387, 427
Wang, L., Dutton, A. A., Stinson, G. S., et al. 2015, MNRAS, 454, 83
Werk, J. k., Prochaska, J. X., Thom, C., et al. 2012, ApJS, 198, 3
Werk, J. k., Prochaska, J. X., Thom, C., et al. 2013, ApJS, 204, 17
Werk, J. k., Prochaska, J. X., Thom, C., et al. 2014, ApJ, 792, 8